Chapter 1

PLASMA MORPHOLOGY AT MARS. ASPERA-3 OBSERVATIONS

E. Dubinin [1], M. Fränz[1], J. Woch[1], E. Roussos [1], S. Barabash[2], R. Lundin [2], J. D. Winningham[3], R. Frahm[3], and M. Acuña[4]

[1]*MPI für Sonnensystemforschung, 37191 Katlenburg-Lindau, Germany*

[2]*Swedish Institute of Space Physics*

[3]*Southwest Research Institute, San Antonio, USA*

[4]*NASA Goddard Space Flight Center, Greenbelt, USA*

Abstract A total of about of 400 orbits during the first year of the ASPERA-3 operation onboard Mars Express spacecraft was analyzed to obtain a statistical pattern of the main plasma domains in the Martian space environment. The environment is controlled by the direct interaction between solar wind and planetary atmosphere/ionosphere which results in the formation of the magnetospheric cavity. Ionospheric plasma was traced by the characteristic "spectral lines" of photoelectrons that make it possible to detect an ionospheric component even far from the planet. Plasma of solar wind and planetary origin was distinguished by the ion mass spectrometry. Several different regions, namely, boundary layer/mantle, plasma sheet, region with ionospheric photoelectrons, ray-like structures near the wake boundary were identified. Upstream parameters like solar wind ram pressure and the direction of the interplanetary electric field were inferred as proxy from the Mars Global Surveyor magnetic field data at a reference point of the magnetic pile up region in the northern dayside hemisphere. It is shown that morphology and dynamics of the main plasma domains and their boundaries are governed by these factors as well as by local crustal magnetization.

Keywords: Mars; magnetosphere, ionosphere, solar wind

1. Introduction

Previous missions to Mars have established the existence of the main plasma regions near Mars. Mariner 4 which passed within $3.9R_M$ of Mars in 1965 has detected a bow shock. At the bow shock solar wind is deflected around Mars. However, as the previous spacecraft (except the Viking landers which have not carried an onboard magnetometer) have not approached Mars closer than $\sim$ 850 km, the nature of the obstacle to the solar wind was not finally resolved before the Mars Global Surveyor (MGS) mission. The MGS measurements have shown that at present Mars does not possess a global intrinsic magnetic field which could be an obstacle for the solar wind as for most of other planets in our solar system (Acuña et al., 1998). Instead, MGS has detected localized, rather strong magnetic anomalies of a crustal origin. Due to the absence of a magnetic obstacle at Mars the solar wind directly interacts with its upper atmosphere and ionosphere and induces a magnetosphere by the pile up of the interplanetary magnetic field. Such an induced magnetosphere can screen the ionosphere from the direct exposure to the solar wind. The formed magnetic barrier separates the solar wind from the ionosphere and acts as an effective obstacle deflecting the magnetosheath plasma. A similar type of interaction occurs around another nonmagnetized planet, Venus, and was extensively explored by the Pioneer-Venus-Orbiter in over 14 years of operation (see, for example, Russell, 1992). Although the PVO mission has provided a wealth of excellent in-situ data about the solar wind/ionosphere interaction for a wide range of solar wind conditions, the plasma component in the energy range $\sim$ 10 eV- 10 keV was studied rather poorly because of instrument and telemetry constraints. The MGS science payload does not include a plasma instrument for the measurement of ion components at Mars, and therefore only the MEX mission and the ASPERA-3 in-situ measurements fill this gap. Paradoxically, there is no magnetometer on MEX.

The most convincing evidence of the formation of the magnetic barrier at Mars was the observations of the magnetic pile up boundary (MPB), a sharp boundary characterized by a strong jump in the magnetic field strength, a drop in the magnetic field fluctuations and a strong decrease in the superthermal electron fluxes (Acuña et al., 1998, Bertucci et al., 2003). Downstream from the MPB, a region called the magnetic pile up region (MPR) is characterized by a sustained high magnetic field. It was believed, despite of a lack of ion measurements on MGS, that the MPB separates the region of shocked solar wind (magnetosheath) from the induced magnetosphere. Such an assumption was supported by the Phobos-2 observations (Breus et. al., 1991, Pedersen et al., 1991, Dubinin et al., 1996). It will be shown subsequently that, indeed, a magnetospheric cavity almost void of the solar wind plasma is formed at Mars.

There is also a somewhat different view. Mitchell et al. (2001) have suggested that another boundary, "ionopause", observed at lower altitudes separates ionospheric and solar wind plasmas. This boundary was detected by the comparison of electron spectra, with magnetosheath-like solar wind electrons above the boundary and ionospheric photoelectrons below the boundary. Its median altitude at solar zenith angles (SZAs) of about 80^0 was estimated as 380 km. "Ionopause" was considered to be a boundary where the ionospheric plasma balances solar wind. However, as it will be shown in this paper, a stoppage of the solar wind occurs at higher altitudes, at the boundary, identified earlier as MPB.

The Martian ionosphere is poorly explored as compared to Venus. The measurements of the main ionospheric characteristics at Mars were made in-situ by the two Viking landers (Hanson et al., 1977, Hanson and Mantas, 1988), that provided us with two ionospheric height profiles, and by radio occultation experiments (Kliore, 1992). Recently new radio occultation and sounding measurements were carried out onboard the MEX spacecraft (Pätzold et al., 2005, Gurnett et al., 2005). The ionosphere of Mars is formed by the photoionization of the major neutral constituents CO_2 and O with subsequent molecular reactions giving rise to O_2^+ as the major ionospheric ion species and O^+ becoming comparable at altitudes ≥ 300 km. Most of the radio occultation profiles show a relatively extended ionosphere without clear ionopause structure. On the other hand, a decrease in the magnetic field value within the ionosphere observed by MGS is a typical feature of the ionopause.

In the ASPERA-3 data, ionospheric plasma is well traced by the characteristic "spectral lines" of photoelectrons which are resolved due to a high energy resolution of the electron spectrometer (Lundin et al., 2004, Frahm et al., 2006). It will be shown here that ionospheric electrons are observed in a wide range of altitudes and the boundary of the photoelectrons (PEB) is often located at higher altitudes than it was reported by Mitchell et al. (2001). It is not clear yet whether PEB and ionopause are collocated since the lowest energy part of the plasma distribution which primary contributes to the thermal pressure has not been measured yet.

It is worth noting that the region below the MPB remains a mysterious one. It will be subsequently shown that the main fluxes of escaping planetary ions are clustered in this region. Energy characteristics of ion beams yield an estimate of electric fields responsible for ion energization. The values of electric field are close to the typical values of the interplanetary motional electric field that implies an effective penetration of solar wind electric field deep into the magnetosphere and effective scavenging of planetary ions (Dubinin et al., 2006a).

The induced magnetosphere contains several different subregions. The boundary layer/mantle dominated by planetary plasma was identified in the previous missions (Vaisberg, 1992, Lundin et al., 1990a, Dubinin et al., 1996). This boundary layer can be considered as a site where the momentum of the solar wind is transferred to the planetary plasma (Lundin et al., 1991, Lundin and Dubinin, 1992). Ray-like structures stretched in the tailward direction were measured on Phobos-2 as well as on the MEX spacecraft (Dubinin et al., 2001, 2006b). It is shown in this paper that both these regions are important channels for the transportation of planetary ions to the tail.

The magnetotail of Mars consists of two lobes of opposite polarity separated by plasma sheet (Yeroshenko et al., 1990). The plasma sheet consists primarily of planetary ions which are accelerated up to keV energies by the magnetic field tensions (Dubinin et al., 1993). The Phobos-2 observations in the tail at distances of $\sim 2.8R_M$ from the planet have revealed signatures of field lines of crustal origin (Dubinin et al., 1994) that implies a complicated magnetic structure of the tail due to reconnection of the IMF and crustal field lines. Large-scale modification of the plasma flow in the tail due to the crustal field contribution was observed in 3D-MHD simulations (Harnett and Winglee, 2005).

Crustal fields add complexity and variability to the Martian magnetic environment (Brain et al., 2003, 2006). The strongest crustal source was detectable up to altitudes of 1300-1400 km and, as it will be shown subsequently, it shifts the magnetospheric boundary upwards (see also Crider, 2004 and Fraenz et al., 2006a). The crustal field also shields the localized regions from intrusion of the magnetosheath plasma (minimagnetospheres) (Fraenz et al., 2006a).

In this paper we have analyzed about 400 orbits during the first year (Feb.-Dec. 2004) of the ASPERA-3 operation onboard the Mars Express spacecraft. In some cases, when we did not use an information about the upstream solar wind and IMF parameters, we have analyzed the observations of two years (2004-2005). MEX ASPERA-3 data provide information about the main plasma domains of the Martian space environment. We present an analysis of the morphology of these regions and their boundaries. We analyze the MGS MAG/ER data to characterize as proxy the upstream conditions, RAM pressure of the solar wind and the direction of the cross flow component of the IMF. We then explore the influence of these parameters on the plasma distribution within the magnetosphere and the position of boundaries. The influence of crustal sources is also studied.

2. Observations

The Mars Express spacecraft was inserted into an elliptical orbit around Mars in January 2004. This eccentric elliptical orbit has a periapsis altitude of about 275 km, an apoapsis of about 10000 km, an orbital inclination of 86^o and a period of 6.75 hours. The scientific payload includes the ASPERA-3 instrument with several sensors to measure electrons, ions and energetic neutral atoms (ENAs). The ASPERA-3 (Analyzer of Space Plasma and Energetic Atoms) experiment is a combination of in-situ and remote diagnostics of atmospheric escape induced by the solar wind. It comprises the Ion Mass Analyzer (IMA), ELectron Spectrometer (ELS), Neutral Particle Imager (NPI) and Neutral Particle Detector (NPD) (Barabash et al., 2004). In this paper we discuss the results obtained from the IMA and ELS sensors. The IMA sensor measures 3D-fluxes of different ion species with m/q resolution (m and q are respectively mass and electric charge) in the energy range 10 eV/q - 30 keV/q with a time resolution of $\sim$ 3 min and a field of view of 90^o x 180^o (electrostatic sweeping provides elevation coverage $\pm 45^o$). Note, that ions with energy less than 300 eV are usually below the measurement threshold. Mass (m/q) resolution is provided by a combination of the electrostatic analyzer with deflection of ions in a cylindrical magnetic field set up by permanent magnets. The ELS instrument measures 2D distributions of the electron fluxes in the energy range 0.4 eV-20 keV ($\delta E/E = 8\%$) with a field of view of 4^o x 180^o and a time resolution of $\sim$ 4 s. In many cases the grid biased at -5 V cuts the low energy ionospheric electrons. A spacecraft potential which is usually positive in solar wind and magnetosheath and negative in a dense ionosphere also strongly influences the measurements in the low energy part of the distribution function. The bulk parameters of plasma were obtained by using algorithms discussed in (Fraenz et al., 2006b).

Figure 1 shows several examples of spectrograms of the electron fluxes which display the different domains of the Martian plasma environment. The dotted curves depict the altitude of the spacecraft over the Mars surface. The respective scale in km is given on the right vertical axes. The corresponding MEX orbits in cylindrical coordinates (with the X-axis directed from the Mars center towards the Sun and the radial distance R taken from the X-axis) are shown in Figure 2. In all these cases the spacecraft subsequently crossed the bow shock, magnetosheath, entered the magnetosphere and moving further along the outbound leg of the orbits recorded all these characteristic regions in the opposite order. The nominal positions of the bow shock (BS) and the magnetic pile-up boundary (MPB) (which can also be referred as the boundary of the induced magnetosphere, MB), determined from the Mars Global Surveyor (MGS) measurements (Vignes et al., 2000) are also given. Pile up of the IMF accompanied by a drop of the solar wind electrons was observed at the MPB (Acuña et al., 1998). The magnetosheath region bounded by the BS and MPB is well displayed in Figure 1 by the appearance of heated at the bow shock solar wind electrons. The cavity void of magnetosheath electrons (the top panel) tell us about the existence of a magnetospheric obstacle to the solar wind. Since Mars has no global intrinsic field the magnetosphere is formed by the pile up of the interplanetary magnetic field (IMF) carried by the solar wind and their draping around the ionospheric obstacle. Indeed, the electron spectra within the Martian magnetosphere contain clear signatures of the ionosphere. The peaks in the electron fluxes near ~ 30 eV appear due to the absorption of the strong solar He II line at 304 $\AA$ in the carbon dioxide dominated atmosphere of Mars (Mantas and Hanson, 1979, Frahm et al. 2006). These peaks can be used for tracing of ionospheric photoelectrons. The interesting feature is that photoelectrons are often observed not only near the periapsis, but also at large altitudes. For example, ionospheric signatures are seen at an altitude of about ~ 900 km, close to the MB on the outbound leg ($\sim$ 0408 UT June 20, 2004). Moreover, traces of "CO_2 photoelectrons" are detected at altitudes up to ~ 5000 km ($\sim$ 0300UT) close to the inbound magnetospheric boundary. In most cases a gap (small or large) exists between the magnetospheric boundary identified by a drop of the sheath electrons and the photoelectron boundary.

New features in the electron fluxes appear within the magnetosphere on the second panel of Figure 1. A spatially narrow plasma structure composed of magnetosheath-like electrons is observed near the wake boundary ($\sim$ 2150 UT). The peak energy of the electrons exceeds their peak-energy at the BS. Plasma in such structures is primarily of planetary origin (O^+ and O_2^+ ions). Different mechanisms were discussed (Dubinin et al., 2006b) to explain the appearance of such structures. One scenario assumes the existence of efficient plasma transport channels into the magnetosphere in magnetic polar regions. In this description the position of the equatorial plane is controlled by the IMF direction, the equatorial plane contains the solar wind velocity and the IMF vector in the undisturbed solar wind. The magnetic field tensions of the draped field lines which become dominant near the MPB (Bertucci et al., 2003) accelerate plasma in the polar regions and push it into the magnetosphere. Such a mechanism suggests a gradual formation of a plasma sheet which separates the two magnetic tail lobes. According to another possible mechanism, reconnection between the crustal and draped IMF field lines can open the inner magnetospheric regions up to solar wind electrons. As a result, magnetic field configurations with "auroral field lines" similar as at Earth, may appear (Lundin et al., 2006).

The appearance of narrow structures near the wake boundary and their stretching in the tailward direction is similar to the features of rays, composed of escaping suprathermal ionospheric O^+ ions, observed at Venus (Brace et al., 1987). Luhmann (1993) suggested that these structures appeared from a thin source region around the terminator where the solar wind convection electric field penetrates into the oxygen-dominated high altitude terminator ionosphere. Dubinin et al. (1991) have also observed such structures in the Martian tail. Most of the events were centered near the wake boundary.

On some orbits, an additional appreciable heating of the sheath electrons is observed in the region adjacent to the magnetospheric boundary (MB) (the third panel from the top in Figure 1, $\sim$ 0355UT). Ion composition measurements show that plasma in such structures consists of planetary O^+ and O_2^+ ions. Figure 3 (the top panel) presents the spectrogram of He^{++} (black curves) and O^+ (red curves) ions. Alpha-particles are used as tracers of the solar wind plasma while oxygen ions have a planetary origin. Planetary ions occupy a broad boundary layer. A similar, although not so appreciable structure is seen on the second panel of Figure 1 at $\sim$ 2130 UT. The bottom panel in Figure 3 depicts normalized to the solar wind conditions the number densities of electrons, protons, atomic (O^+) and molecular (O_2^+) oxygen ions, and the electron temperature. Electron heating and a density increase associated with the appearance of planetary ions near the magnetospheric boundary (MB) at 0312 UT is observed. A change of the ion composition in the boundary layer/mantle is the characteristic feature of the transition. Another structure observed at $\sim$ 0340, near the wake boundary, is similar to the ray structure seen on the second panel. Similar observations by the Phobos-2 spacecraft have suggested that the magnetospheric boundary at Mars is also the ion composition boundary to emphasize a sharp transition from the solar wind to planetary plasma. As a matter of fact, all these boundaries at a macroscopic scale are collocated in the same position (Dubinin et al., 1996, Nagy et al., 2004).

Pioneer-Venus-Orbiter observations made at another nonmagnetized planet, Venus, have shown the existence of the boundary layer with enhanced wave activity (Perez-de-Tejada et al., 1993). Its appearance was attributed to a "friction" action between the shocked solar wind and planetary plasma (Perez-de-Tejada, 1979). Although the terms "viscosity" and "friction" are not well determined in a collisionless plasma, dissipative processes associated with the transport of the solar wind momentum to the planetary plasma could be responsible for the observed electron heating.

The fourth panel in Figure 1 demonstrates the existence of a boundary layer with an additional heating of magnetosheath electrons on the outbound leg of the orbit ($\sim$ 1725 UT) when the spacecraft crossed the near terminator magnetopause. Figure 4 presents the normalized number densities of electrons, protons, atomic (O^+) and molecular (O_2^+) oxygen ions, and the electron temperature. Note here, that the boundary layer (mantle) composed of planetary ions is not always accompanied by appreciable electron heating as for the outbound crossing (1832UT) (see, for example, the inbound crossing at 1632 UT). The inconsistency between the electron and ion number densities in the inbound magnetosphere (after 1632UT) is due to the instrumental "gaps" in the measurements of the low-energy parts of the electron and ion distributions.

The above examples display the different characteristic features of the main plasma regions which were used to trace and explore their morphology.

Magnetospheric boundary

We have analyzed the position of the magnetospheric boundary characterized by a drop of the magnetosheath electrons using MEX-ASPERA-3 data from February 2004-December 2004. Figure 5 presents the position of the boundary crossings plotted in cylindrical coordinates. Superposed on the data points red and blue curves depict the position of the bow shock and magnetic pile up boundary from Vignes et al. (2000) (MGS data) and the bow shock and planetopause (PP) from Trotignon et al. (1996) (Phobos-2 data), respectively. Different names of boundaries introduced from single instrument observations, as a matter of fact, correspond to the same and one magnetospheric boundary (Dubinin et al., 1996, Nagy et al., 2004). It is observed that at small solar zenith angles the position of the boundary is closer to the planet and in a better agreement with the PP position derived from the Phobos-2 measurements although the solar activity during these missions was very different (Figure 6). In contrast, at larger solar zenith angles, the positions of the magnetospheric boundary (MB) and MPB are in a reasonable agreement. The used equation of the MPB surface (in assumption of a cylindrical symmetry along the X-axis) in polar coordinates was (Vignes et al., 2000)

$$r = \frac{L}{1 + \epsilon \cos\theta}. \tag{1.1}$$

Here $L = 0.96R_M$ and $\epsilon = 0.9$ are the semi-latus tectum and the eccentricity, respectively. Polar coordinates (r, θ) are measured about the focus located at the point $(x_0 = 0.78, 0, 0)$. A better agreement with the MEX-ASPERA-3 observations, in particularly, at small solar zenith angles can be obtained by using the same values for L and ϵ, but moving the focus to $x_0 = 0.7$ (the dotted black curve in Figure 5).

Figure 5 also shows that a scatter of the data points with respect to the nominal boundary position, increases with the solar zenith angle.

The boundary determined from a drop of the magnetosheath electrons coincides with a boundary of a "stoppage" of the solar wind. Figure 7 compares the median distributions of fluxes of the $E_e = 80 - 100$ eV electrons and the number densities of He^{++} ions. The data set contains the measurements carried out by ASPERA-3 over two years (2004-2005). The magnetosphere almost void of solar wind particles can well be seen. Since the magnetic pile up boundary is also characterized by a drop of the magnetosheath electrons, MPB is the magnetospheric, obstacle boundary which determines the position of bow shock and plasma flow around Mars. We used here a simple definition of the magnetospheric boundary, MB, because of the lack of the magnetic field measurements on MEX.

The existence of an extended magnetospheric cavity for median conditions does not imply that solar wind can not penetrate to closer altitudes above the planet. Magnetospheric "images" plotted for maximum values of fluxes and densities in each bin reveal a significant contraction of the magnetosphere (not shown here) for extreme conditions in the solar wind. Among the main factors which are expected to account for the observed variations of the boundary position are the solar wind dynamic pressure, local crustal magnetic field sources and orientation of the interplanetary electric field $-\boldsymbol{V}_{sw} \times \boldsymbol{B}_{IMF}$.

Solar wind dynamic pressure dependence. In this paper we use a MGS proxy for the solar wind RAM pressure monitoring. It is assumed that the solar wind dynamic pressure is balanced at the induced magnetospheric boundary (MPB) by the magnetic field pressure of the draped IMF tubes. The pileup of the magnetic field and formation of the induced magnetic barrier occurs over a short distance, that accounts for a sudden drop of the solar wind electron and proton fluxes. The magnetic field value remains approximately constant for several hundred km in the magnetic pile up region (MPR) (Crider et al., 2003). On mapping orbits, the MGS spacecraft moves along a circular 0200-LT/1400-LT polar trajectory at the altitude of ~ 400 km, crossing the MPR in the northern hemisphere. Since the magnetic field at middle latitudes of the northern hemisphere is primarily of induced origin, we can use its value as a proxy for the magnetic field pressure which stops the solar wind, and readily infer a proxy value for the solar wind dynamic pressure

$$kP_{dyn}\cos^2\theta = \frac{B^2}{2\mu_o}, \tag{1.2}$$

where $k \sim 0.88$ and θ is the solar zenith angle and the magnetic field B is measured on each MGS orbit on the dayside at the reference point $\theta \sim 45^o$. This proxy solar wind dynamic pressure P_{dyn} is adjusted to the times of the magnetosheath boundary crossings. It is worth noting that Vennerstrom et al. (2003) and Crider et al. (2003) have also successfully used the MGS data as a proxy for solar wind pressure.

Figure 8 compares variations of the inferred solar wind dynamic pressure and the ratio r_{obs}/r_{ave} which characterizes the difference in the measured and averaged boundary positions. Here r_{obs} is the length of the radius-vector between the focus point $(x_o, 0, 0)$ and the observation point of the MB, and r_{ave} is the distance from the focus to the crossing point of the average boundary surface and the vector $\boldsymbol{r}_{obs}$. The MEX data are separated on two groups of $R_{obs} > 1.4R_M$ and $R_{obs} < 1.4R_M$, where R_{obs} is the radial distance from the X-axis to the observation point. The small $R_{obs} < 1.4R_M$ group corresponds to solar zenith angles less than $60 - 70^o$. It is observed that the response of the boundary position to the RAM pressure is better visible at smaller zenith angles. The dashed curves in Figure 8 show a power law ($P_{dyn}^{-1/6}$) dependence. Verigin et al (1993) have shown that the diameter of the Martian tail D is proportional to $P_{dyn}^{-1/6}$ what is expected if Mars would have an intrinsic magnetosphere. A similar dependence was noted by Dubinin et al. (1996) although the authors have argued in a favor of an induced magnetosphere. For the small R_{obs} group a power law fit is given by $r_{obs}/r_{ave} \sim P_{dyn}^{-0.053}$ that is in a good agreement with the MGS data, $k = -0.0546$ (Crider et al., 2003). If we exclude the data points for small values of the RAM pressure ($P_{dyn} > 0.133$ nPa) then the power law index $k \sim -0.083$ (the dotted curve in Figure 8a). For the large R_{obs} group, the index $k = -0.065$ (the dotted curve in Figure 8b).

Thus the MEX data as well as the MGS observations show a weaker dependence between the RAM pressure and variations in the MB location than it is expected for a magnetic dipole obstacle. Nevertheless a power law dependence is still revealed. Such dependence becomes weaker and ceases for small P_{dyn} that is better seen in Figure 9 which depicts the r_{obs}/r_{ave} as a function of $P_{dyn}^{-1/6}$. It is interesting to note, that although now there is no a solid argument to expect the power law index $k = -1/6$ for the induced magnetospheric obstacles, Brecht (1995) have observed a similar dependence of the magnetotail width on the RAM pressure in hybrid simulations of the solar wind interaction with "nonmagnetized" Mars. While comparing the Phobos-2 and MGS, MEX observations it is also necessary to recall that solar wind pressure in the Phobos-2 data has been measured in-situ. On the other hand, the sampling of the Phobos-2 data was poorer.

Interplanetary electric field dependence. For the study of the solar wind interaction with planets like Mars or Venus having draped magnetospheric configurations, the IMF reference frame is the most sensible one. This coordinate system has the X^*-axis antiparallel with the upstream solar wind flow and Y^*-axis along the cross-flow magnetic field component of the IMF. Then the motional electric field $-\boldsymbol{V}_{sw} \times \boldsymbol{B}_{IMF}$ is always along the Z^*-axis. Since there is no magnetometer on the MEX spacecraft the only way to infer an information about the IMF is the MGS observations in the MPR. Assuming that the clock-angle of the IMF is not changed while the field lines are draped around Mars we can infer a proxy direction of the cross-flow magnetic field component and construct the IMF coordinate system. We used the same reference point in the dayside northern hemisphere as for the determination of a proxy RAM pressure. As a matter of fact, the IMF system is inadequate to observe simultaneously in two dimensions a possible "north-south" asymmetry due to the motional electric field and a "dawn-dusk" draping asymmetry, if both sector polarities of the IMF are analyzed. Moore et al. (1990) have used a combination of rotations and foldings (see also Dubinin et al., 1996). However, in our case, the lack of information about the X-component of the IMF does not allow to apply the foldings. Normalizing a boundary position to average solar wind conditions ($P_{dyn} = 1nPa$) by using the power law fit dependence we can test a possible asymmetry of the magnetosphere in the IMF coordinate plane. Figure 10 shows r_{obs}/r_{ave} in the plane Y^*Z^*. We observe only a certain elongation of the magnetospheric shape in the "north-dawn" direction for $R_{obs} > 1.4R_M$ probably caused by two factors: (i) a preferential pile up of the IMF in the "northern" hemisphere and (ii) a "dawn-dusk" asymmetry of the draping due to X-component of the IMF.

Observations near Venus have shown that the piled up magnetic field is stronger in the Z^*-hemisphere into which the motional electric field is pointing (Luhmann et al., 1985). A similar effect is found at Mars (Vennerstrom et al., 2003) as well as in 3-D hybrid simulations of the solar wind interaction with Mars (Bößwetter et al., 2004, Modolo et al., 2005). Therefore it is could be expected that the position of the magnetospheric boundary is further from the planet in the $+Z^*$-hemisphere. However this effect is not visible in our data set.

Crustal field dependence. The crustal magnetic fields can also influence the position of the magnetospheric boundary as the magnetic pressure in some localized regions may be high enough to balance the solar wind dynamic pressure. Crider et al. (2002) have found that the MPB distance increases with increasing southern latitude. Using the electron measurements by ASPERA-3-ELS, Fraenz et al. (2006a) have shown that the altitude of the intruded magnetosheath electrons ($E_e = 80 - 100$eV) increases with the strength of the crustal field. Figure 11a shows a relative shift of the boundary in the dayside southern hemisphere with respect to its averaged position (r_{obs}/r_{ave}) as a function of the strength of the crustal magnetic field. We used the crustal field strength interpolated on a regular grid for an altitude of 400 km from the MGS MAG/ER observations as presented by Connerney et al. (2001). Although the sampling of measurements above the strong crustal sources is small an upward motion of the boundary with increasing magnetic field strength is clearly observed. There is a reasonable agreement with the picture of the intrusion of magnetosheath electrons as a function of crustal field strength (Figure 11b).

Ionospheric photoelectrons

The ionospheric electrons are well traced by the peaks in the energy spectra of the electrons in the range of 20-30 eV. Observations of such electrons can be used to probe the Martian ionosphere. Figure 12 compares the position of the magnetospheric boundary R (R is the radial distance from the X-axis) with the radial distances at which the characteristic "CO_2-lines" in the photoelectron spectra were observed. Diamond-shaped points correspond to the boundary crossings on inbound and outbound legs of the MEX orbit in 2004. Crossings occur at different radial distances due to the orbit evolution. Two groups of MB locations, nearby and distant are clearly revealed. Red segments depict the radial distances along the orbital intervals on which ionospheric photoelectrons were observed. It is seen that the photoelectrons are always detected close to the nearby MB almost filling the whole dayside magnetosphere. In many cases the photoelectrons are also observed close to the distant positions of the magnetospheric boundary.

Figure 13 shows the distribution of the energy flux of "CO_2" - photoelectrons in the energy range ($\delta E = 4$ eV) centered near its characteristic "spectral lines" (20-30 eV) in cylindrical coordinates. Floating of these spectral peaks due to spacecraft potential variations was taken into account. The ionospheric electrons are observed at altitudes up to $\sim$ 7000 km. Another interesting feature is that the photoelectrons are detected close to the nominal magnetospheric boundary - that implies an important role of the ionospheric plasma as an obstacle to solar wind. Unsolved yet is the question, does a drop of photoelectrons near the magnetospheric boundary correspond to the ionopause?

According to the MGS aerobraking observations (Mitchell et al., 2000) at solar zenith angles (SZAs) $\sim 80^o$ the ionopause was crossed in the altitude range 180-800 km with a median value of 380 km. The ionopause was identified by a drop of the electron fluxes above $\sim$ 100 eV. The electron spectrometer (ELS) of the ASPERA-3 experiment due to a higher energy resolution was able to identify the boundary of photoelectrons with a better accuracy as a position where fluxes of CO_2-photoelectrons cease. In contrast, a drop of the magnetosheath electrons ($E_e = 100$eV) on the dayside approximately coincides with the magnetospheric boundary (MB).

Recall that the term ionopause was introduced to describe the direct interaction between the solar wind plasma and ionosphere at Venus. The currents flowing in the thin layer (ionopause), where the external hot solar wind magnetized plasma and cold ionospheric plasma balance each other, screen the magnetic field from the ionosphere. They cause a pileup of magnetic field lines in front of the ionopause. A magnetic field barrier of piled up field lines almost balances the solar wind pressure. On the other hand, the magnetic field pressure balances the thermal ionospheric pressure at lower altitudes. As a result, the real obstacle to the solar wind is observed at the magnetic barrier whose position is further from the planet than the ionopause (see, for example, Zhang et al., 1990). If the ionosphere is resistive the ionopause is broadened and the magnetic field penetrates deeper into the ionosphere. This happens, for example, when the solar wind pressure increases and the ionopause moves to lower altitudes where there are more collisions between particles.

In the Martian case, the magnetic pile up boundary accompanied by a drop of solar wind particles (ions and electrons) can be also considered as an obstacle boundary to the solar wind (although, as a matter of fact, a pressure balance at Mars was not tested yet). The photoelectron boundary (PEB) determined by a drop of "CO_2"-photoelectrons is located at slightly lower altitudes. There is some uncertainty about the position of the ionopause if we speak in terms of pressure balance.

Reliable ionospheric profiles near the MPB are absent. Recent MARSIS ionospheric soundings (Gurnett et al., 2005) performed on MEX have shown that the ionospheric number density at altitude of ~ 400 km near the terminator is about of $3 \cdot 10^3 cm^{-3}$. That implies a possible essential contribution to the pressure balance at altitudes of the magnetospheric boundary. However, it is unlikely that the ionospheric pressure at PEB altitudes is able to stop the solar wind. We may assume that some part of the momentum of the solar wind can be transferred to the ionosphere via the magnetic field stresses driving the ionospheric plasma into motion. This motion can explain the observations of ionospheric photoelectrons far in the tail. The photoelectrons can also lift up along the magnetic field lines and, particularly, along the reconnected crustal field lines which are stretched into the tail ("polar wind" at Mars). Since the motion of low-energy ionospheric plasma is not quantified yet it is difficult to estimate escape fluxes of oxygen from the topside ionosphere.

Figure 14 presents the fluxes of "CO_2"-photoelectrons in the IMF coordinate system. A small bulge in the $(-Y^* + Z^*)$ - hemisphere is similar to a bulge in the position of the magnetospheric boundary (Figure 10) implying a contribution of the ionospheric plasma to the formation of the obstacle. The observed "dawn-dusk" asymmetry can be caused by different tension forces of the draped field lines due to the presence of the X-component of the IMF.

Ray structure near the wake boundary

The ASPERA-3 experiment has often observed a spatially narrow structure composed of hot sheath-like electrons and planetary ions near the wake boundary (see the second and third panels in Figure 1 and Dubinin et al., 2006b). The structure appears near the terminator plane and is stretched, like a ray into the tail. Figure 15a shows in $R - X$ coordinates locations of the events observed in 2004. Figure 15b gives the image of electron fluxes in the energy range of 80-100 eV along the orbits on which ray-electron structures were observed. Such rays are important erosion channels through which planetary ions are transported to the tail. That can be readily inferred from Figure 15c which shows density fluxes of oxygen ions along the same set of MEX orbits. It was suggested (Dubinin et al., 2006b) that draped field lines slipping along the magnetospheric surface near the MPB, around the "magnetic poles" can push planetary ions into the magnetosphere. This mechanism also explains the formation of the plasma sheet which separates two magnetic field lobes in the induced tail. Recent hybrid simulations (Bößwetter et al., 2004, Modolo et al., 2005) have shown a distinct asymmetry in the strength of the field at the MPB. The maximum intensity of the draped magnetic field is observed in the hemisphere into which the motional electric field is pointing (the "northern" hemisphere in the IMF coordinate system). Therefore, if this mechanism works, one would expect a preferential observation of ray structures in the $+Z^*$ hemisphere near the pole. Figure 16a depicts the locations of the orbital segments along which ray-events were observed in the IMF Y^*Z^*-plane. It is seen that most of the events are clustered near the "northern magnetic pole". There are also events near the "magnetic equator" which could be the counterparts of stretched ray-like structures in the "magnetic equatorial plane" observed in 3D-hybrid simulations (Bößwetter et al., 2004, Modolo et al., 2005). A mechanism which pushes planetary ions along the field lines is probably related to a day-night pressure gradient. The asymmetry of ray structures is also revealed on the right panel in Figure 16b which shows the fluxes of oxygen ions along the orbits in which the ray features were observed in the electron data.

Another mechanism which associates the events with auroral inverted "V" structures suggests their appearance in the southern hemisphere where the shear flows at the boundary of open, draped IMF field lines and closed field lines from crustal sources can generate field-aligned currents and the parallel electric fields. Figure 16c depicts the maximum fluxes of the 80-100 eV electrons in the ring-area $(0.7 - 1.3R_M)$ during two years. The fluxes near wake boundary dominate in the southern hemisphere. Thus both mechanisms probably contribute to the occurrence of ray-like structures.

Boundary layer and Plasma sheet

Another important reservoir of planetary ions is the boundary layer. The existence of the boundary layer/mantle in the Martian magnetosphere has been shown during the first Soviet space missions to Mars (Vaisberg 1992) as well as in the Phobos-2 observations (Lundin et al.,1990a, Breus et al., 1991, Dubinin et al., 1996). Moreover, it was assumed that the boundary layer is a main channel for the escape of planetary ions (Lundin et al., 1990b). Figure 17 (left panel) shows in the $R - X$ plane the orbital segments near the MB along which planetary ions were detected. The right panel depicts the values of oxygen ion fluxes measured during these intervals. The main fluxes are observed within the magnetosphere although on some orbits remarkable fluxes of planetary ions were also recorded in the adjacent magnetosheath. The values of fluxes in the boundary layer often exceed $10^7 cm^{-2}s^{-1}$.

The geometry of the outflowing plasma is very important for calculations of the total escape rate of planetary matter. Analyzing the ASPERA data on Phobos-2 Lundin et al. (1989, 1990b) have suggested that a primary solar wind induced escape with a total rate of about $2.5 \times 10^{25} s^{-1}$ occurs through a cylindrically symmetric boundary layer. Verigin et al. (1991) have made the assumption that the main channel for the loss of planetary ions is the plasma sheet. Correspondingly, the estimated total outflow rate in this case is significantly less ($\sim 5 \times 10^{24} s^{-1}$). Figure 18 presents the data set of the observations made in the boundary layer with ASPERA-3 on MEX in the IMF coordinate system. A strong "dawn-dusk" asymmetry is probably related with the draping in both hemispheres. If we assume that planetary oxygen ions emanate from an asymmetric ring-shaped area $0.8R_M$ in thickness around the terminator and typical fluxes of ions are of the order of $\sim 10^6 - 10^7 cm^{-2} s^{-1}$, the total escape rate would be about $6 \times 10^{23} - 6 \times 10^{24} s^{-1}$. Recall here, that the MEX measurements were carried out close to solar minimum conditions while the Phobos-2 spacecraft has operated near Mars at solar maximum when the oxygen exosphere was expected to be denser. Perhaps, these estimates may be still revised since (i) the boundary layer was observed only in $\sim 20 - 25\%$ of the magnetosphere crossings; (ii) in-flight calibration of the IMA sensors may change the values of ion fluxes. The absence of the boundary layer in $\sim 80\%$ of cases implies that there are probably other, unknown yet factors, than the geometry of the IMF, which control the escape processes.

It was observed (see Section 1) that on some orbits the boundary layer is characterized by a sudden additional heating of magnetosheath electrons. Spectra of electrons in these cases become similar to the spectra observed in ray-structures or in the plasma sheet. The ion composition is dominated by O^+ and O_2^+ ions. A change of ion composition of the plasma within these structures implies that the observed spikes of heated electrons at the inner edge of the sheath are not related to temporal variations in the magnetosheath caused by the passage of different types of inhomogeneities and discontinuities in the solar wind, but that they are an inherent boundary layer feature. Figure 19 shows the position of sample events in cylindrical coordinates. The corresponding spectrograms of electron fluxes with clear spikes of electron heating near the MB are also shown. The inner part of the magnetosphere is readily recognized by the absence of magnetosheath-like electrons. The positions of the bow shock (BS) and the boundary events (BE) are also marked. In IMF coordinates the BEs appear in the $+Z^*$-hemisphere. More analysis is required to understand the origin of these events.

The magnetosphere structure within the optical shadow of Mars ($R < 1R_M$) is still poorly covered by the ASPERA-3 measurements. The observations of the plasma sheet carried out in 2004 yield a similar morphological pattern as for the ray-structures (see Figures 15 and 16) which may imply that they have a common root. The values of oxygen fluxes in the plasma sheet are somewhat higher than in the boundary layer and often exceed $10^7 cm^{-2} s^{-1}$.

Blue and green segments in Figure 11 depict the radial distances along the orbital intervals on which fluxes of planetary ions were observed in the boundary layer and plasma sheet, respectively. It is seen that these fluxes together with ionospheric photoelectrons almost entirely fill the whole magnetosphere from the MB to periapsis altitudes.

3. Summary

We explored the morphology of the main plasma regions and their boundaries by analyzing MEX ASPERA-3 data collected in 2004.

1. It is shown that a magnetospheric cavity strongly depleted in solar wind particles is formed. The position of its boundary determined by a drop of fluxes of ~ 100 eV magnetosheath electrons coincides with a boundary determined by a drop of solar wind ions. This implies that the magnetospheric boundary is collocated with the MPB which is also characterized by a drop of the magnetosheath electrons.

2. We have analyzed the position of the magnetospheric boundary and compared it with Phobos-2 and MGS observations. Good agreement with Phobos-2 observations at small solar zenith angles and with MGS data for larger angles is observed. A general reasonable agreement in the MB position observed at different phases of solar activity implies that it is not sensitive to this parameter. A similar conclusion was made by Vignes et al. (2000) while comparing the Phobos-2 and MGS data.

3. Variations in the MB location increase with increasing SZA.

4. We have analyzed the dependence of MB locations on solar wind dynamic pressure. We used a MGS proxy for solar wind RAM pressure assuming that the RAM pressure is balanced at the MPB by the magnetic field pressure. It is generally observed that variations of the MB position are in a reasonable agreement with a magnetic origin of the obstacle to the solar wind. It is shown that a response of the MB to the RAM pressure is revealed more clearly at SZA $\leq 60^o - 70^o$. The K-H instability of shear flows near the MB may result in large inward-outward motions of the MB at larger zenith angles providing a significant "scattering" in the MB locations.

5. The ASPERA-3 data show a weaker power law dependence between the RAM pressure and variations in the MB location than it is expected for a magnetic dipole obstacle.

6. In the IMF coordinate system, determined by the cross-flow component of the IMF, a "north-south" asymmetry in the MB location caused by mass loading effect in the electric field pointing hemisphere is not found. A certain elongation observed in the "dawn-north" direction is probably due to an asymmetry of the draping.

7. Although the sampling of MB measurements above strong crustal source is poor, an upward lift of the MB is observed. This trend is also confirmed by an altitude-crustal field dependence of protrusion of magnetosheath electrons.

8. Ionospheric photoelectrons traced by their characteristic peaks in energy spectra are used to identify the photoelectron boundary PEB and explore their distribution within the Martian magnetosphere. Photoelectrons can be observed close to the MB locations implying an important role of the ionospheric component in dynamic processes responsible for the formation of the magnetospheric obstacle at Mars. It is unlikely that PEB and ionopause (as a pressure balance boundary) are collocated. It is assumed that some part of the momentum from solar wind is transferred to the ionosphere driving it into a convective motion. This motion together with a mechanism of "polar wind' along "open" field lines can explain the observation of ionospheric photoelectrons at distances more than $3R_M$ far in the tail.

9. In the IMF reference frame the distribution of photoelectrons reveals a similar asymmetry as the magnetospheric boundary.

10. It is shown that the position of ray-like structures centered close to the wake boundary are governed by the IMF direction. The events are clustered in the hemisphere of locally convective electric field. This supports the suggestion that these structures are formed in a process of scavenging of planetary plasma by draped magnetic field lines near the "magnetic poles". However their dominance in the southern hemisphere also implies a possible important role of auroral-like acceleration processes at Mars. A "dawn-dusk" asymmetry due to draping features is also revealed.

11. It is shown that the boundary layer/mantle is an important channel for planetary ions escaping from the Martian space. A strong "dawn-dusk" asymmetry in IMF coordinates appeared due to a draping asymmetry. Estimates of outflowing fluxes of oxygen ions yield $6 \times 10^{23} - 6 \times 10^{24} s^{-1}$. However, these values may be somewhat revised after the final instrumental calibration.

12. Plasmas of ionospheric and atmospheric origin which fill the region between MB and ionopause are not in a static pressure equilibrium with solar wind, but driven into a convective motion.

13. An interesting class of events is observed close to the inner boundary of the magnetosheath. These boundary events are characterized by an abrupt additional heating of magnetosheath electrons and remarkable fluxes of planetary ions. It is not clear yet whether such events are the manifestation of a transition, "viscous-like" layer as observed near Venus or crossings of a plasma sheet near the MB.

Acknowledgments

The ASPERA experiment on the European Space Agency (ESA) Mars Express mission is a joint effort between 15 laboratories in 10 countries, all sponsored by their national agencies as well as the various departments/institutes hosting these efforts. We wish to acknowledge support from Deutsche Forschungsgemeinschaft for supporting this work by grant WO 910/1-1 and DLR grant 50QM99035. We also wish to acknowledge the Swedish National Space Board for their support of the main PI-institute and we are indebted to ESA for their courage in embarking on the Mars Express program, the first ESA mission to the red planet. We wish to acknowledge support of NASA contract NASW00003 for the support of the design, construction,operation for the Electron Spectrometer through the Discovery Program Mission of Opportunity.

References

Acuña, M. H., Connerney, J., Wasilewski, P. et al.: 1998, Science 279, 5357, 1676.

Barabash, S., Lundin, R., Andersson H. et al.: 2004, ESA publication SP-1240, 121.

Bertucci, C., Mazelle, C., Crider D. et al.: 2003, Geophys. Res. Lett., 30, 1876, doi:10.1029/2002GL015713.

Bößwetter, A., Bagdonat, T., Motschmann, U., Sauer, K.: 2004, Annal. Geophys. 22(12), 4363.

Brace, L. H., Kasprzak, W. T., Taylor, H. A., Theis, T. F., Russell, C. T., Barnes, A., Mihalov, J. D., Hunten, D. M.: 1987, J. Geophys. Res. 92, 15.

Brain, D. A., Bagenal, F., Acuña, M. and Connerney, J. E.: 2003, J. Geophys. Res., 108(A12), 1424, doi:10.1029/2002JA009482.

Brain, D. A., and Mitchell, D. L.: 2006, Icarus, in press.

Brecht, S. H.: 1995, Geophys. Res. Lett., 22, 1181.

Breus, T., Krymskii, A., Lundin, R. , Dubinin E. et al.: 1991, J. Geophys. Res., 96, 11165.

Connerney, L. E., Acuña, M. ,Wasilewski, P., Kletetschka, G., Ness, N. F., Reme, H., Lin, R., and Mitchell, D.: 2001, Geophys. Res. Lett, 28, 4015.

Crider, D. H., Vignes, D., Krymskii, A., Breus, T., Ness, N., Mitchell, D., Slavin, J., and Acuña, M.: 2003, J. Geophys. Res., 108(A12), 1461, doi:10.1029/2003JA009875.

Crider, D. H.: 2004, Adv. Space Res., 33, 152.

Dubinin, E., Lundin, R., Riedler, W., Schwingenschuh, K., Luhmann, J., Russell, C. T., and Brace, L. H.: 1991, J. Geophys. Res., 96, 11189.

Dubinin, E., Lundin, R., Koskinen, H., and Pissarenko, N.: 1993, J. Geophys. Res., 98, 3991.

Dubinin, E., Lundin, R., and Schwingenschuh K.: 1994, J. Geophys. Res., 99, 21233.

Dubinin, E., Sauer, K., Lundin, R., Norberg, O., Trotignon, J.-G., Schwingenschuh, K., Delva, M., and Riedler, W.: 1996, J. Geophys. Res., 101, 27061.

Dubinin, E., Winningham, J. D., Fraenz, M., Woch, J. et al.: 2006a, Icarus, in press.

Dubinin, E., Winningham, J. D., Fraenz, M., Woch, J. et al.: 2006b, Icarus, in press.

Fraenz, M., Winningham, J. D., Dubinin, E., Roussos, E. et al.: 2006a, Icarus, in press.

Fraenz, M., Dubinin, E., Roussos, E. J. Woch.: 2006b, Space Sci. Rev., this issue.

Frahm, R., Winningham, J. D. et al.: 2006, Icarus, in press.

Gurnett, D. A., Kirchner, D. L., Huff, R. L., Morgan D. et al.:2005, Science, 310, 1929.

Hanson, W. B., Sanatani, S., and Zuccaro, D. R.: 1977, J. Geophys. Res., 82, 4351.

Hanson, W. B., and Mantas, G. P.: 1988, J. Geophys. Res., 93, 7538.

Harnett, E. M. , and Winglee, R. M.: 2005, J. Geophys. Res., 110, A07226, doi:10.1029/2003JA010315.

Kliore, A. J.: 1992, in: J. G. Luhmann, M. Tatrallyay, R. O. Pepin, (eds), Venus and Mars: Atmospheres, Ionospheres and Solar Wind Interactions, AGU monograph 66, Washington, DC, p. 265.

Luhmann, J. G., Russell, C. T., Spreiter, J. R., and Stahara, S. S.: 1985, Adv. Space Res., 5(4), 307.

Luhmann, J. G.: 1993, J. Geophys. Res. 98, 17615.

Lundin, R., and Dubinin, E.: 1992, Adv. Space Sci., 12(9), 255.

Lundin, R., Zakharov, A., Pellinen R., et al.: 1989, Nature 341, 609.

Lundin R., Zakharov, A., Pellinen, R. et al.: 1990a, Geophys. Res. Lett, 17, 873.

Lundin, R., Zakharov, A., Pellinen, R. et al.: 1990b, Geophys. Res. Lett. 17, 877.

Lundin, R., Dubinin, E., Koskinen, H., Norberg, O., Pissarenko, N., and Barabash, S.: 1991, Geophys. Res. Lett., 18, 1059.

Lundin, R., Barabash, S. , Andersson, H. et al.: 2004, Science 305, 1933.

Lundin, R., Winningham, J. D., Barabash, S. et al.: 2006, Science, 311, 980.

Mantas, G. P., and Hanson, W. B.: 1979, J. Geophys. Res., 84, 369.

Mitchell, D. L., Lin, R. P., Mazelle, C. et al.: 2001, J. Geophys. Res. 106, 23419.

Modolo R., Chanteur, G., Dubinin, E., Matthews, A.: 2005, Annal. Geophys. 23, 433.

Moore, K. R., McComas, D., Russell, C. T. , and Mihalov, J. D.: 1990, J. Geophys. Res., 95, 12005.

Nagy, A. F., Winterhalter, D., Sauer, K. et al.: 2004, Space Sci. Rev. 111(1), 33.

Pätzold, M., Tellmann, S., Häusler, B., Hinson, D., Schaa, R., and Tyler, G. L.: 2005, Science, 310, 837.

Pedersen, A, Nairn, C., Grard, R., and Schwingenschuh, K.: 1991, J. Geophys. Res., 96, 11243.

Perez-de-Tejada, H.: 1979, J. Geophys. Res., 84, 1555.

Perez-de-Tejada, H., Intriligator, D. S., and Strangeway, R. J.: 1993, Geophys. Res. Lett., 20, 991.

Russell, C. T.: 1992, in: J. G. Luhmann, M. Tatrallyay, R. O. Pepin, (eds), Venus and Mars: Atmospheres, Ionospheres and Solar Wind Interactions, AGU monograph 66, Washington, DC, p. 225.

Smith, E. J., Davis, L. , Coleman, P.L. and Jones, D. E.: 1965, Science, 149, 1241.

Trotignon, J.-G., Dubinin, E., Grard, R., Barabash, S. and Lundin, R.: 1996, J. Geophys. Res., 101, 24965.

Vaisberg, O.: 1992, in: J. G. Luhmann, M. Tatrallyay, R. O. Pepin, (eds), Venus and Mars: Atmospheres, Ionospheres and Solar Wind Interactions, AGU monograph 66, Washington, DC, p. 311.

Verigin, M., Shutte, N., Galeev, A., Gringauz K. I. et al.: 1991, Planet. Space Sci., 39., 131.

Verigin, M. et al.: 1993, J. Geophys. Res., 98, 1303.

Vennerstrom, S. Olsen, N., Purucker, M., and Acuña, M.: 2003, Geophys. Res. Lett., 30(7), 1369, doi:10.1029/2003GL016883.

Vignes. D., Mazelle, C., Reme, H., Acuña, M. et al.: 2000, Geophys. Res. Lett. 27, 49.

Yeroshenko, Ye. Riedler, W. R., Scwingenschuh, K., Luhmann, J. G., Ong, M., and Russell, C. T., Geophys. Res. Lett., 17, 885.

Zhang, T. L., Luhmann, J. G., Russell, C. T.: 1990, J. Geophys. Res. 81, 1636.

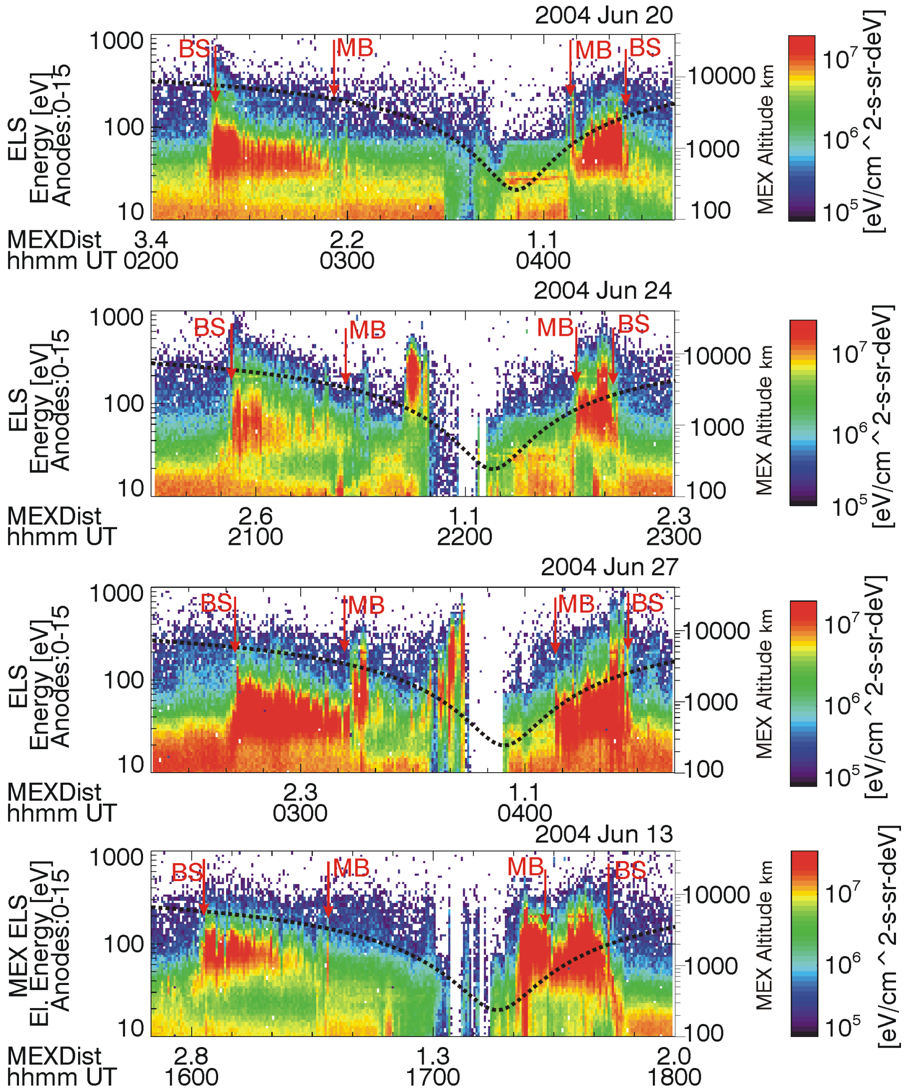

Figure 1.1. (top) Spectrograms of electron fluxes along the several similar MEX orbits. Dotted curves show the MEX altitude (scale in km is given on the right vertical axis). Positions of the bow shock (BS) and magnetospheric boundary (MB) are marked by arrows.

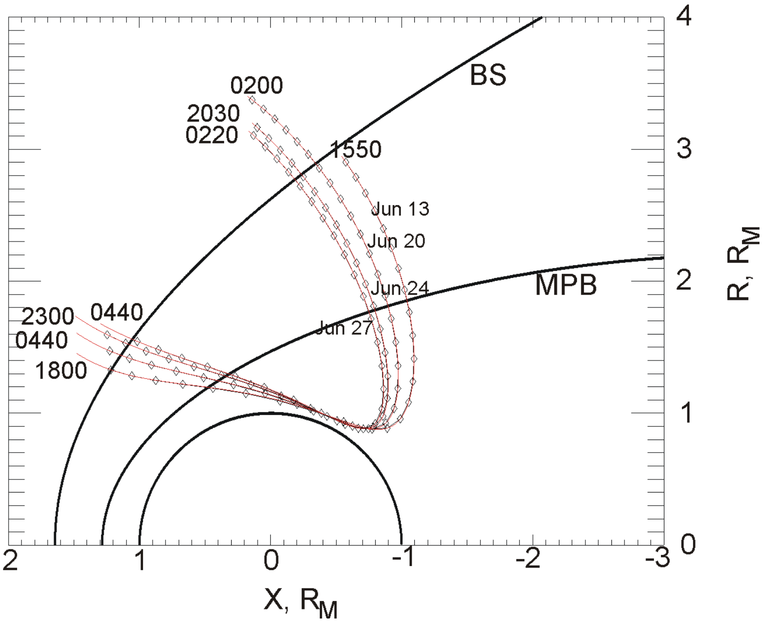

Figure 1.2. Orbits of MEX in cylindrical coordinates. The spacecraft enters the magnetosphere at $X \sim -1R_M$ and exits near the terminator.

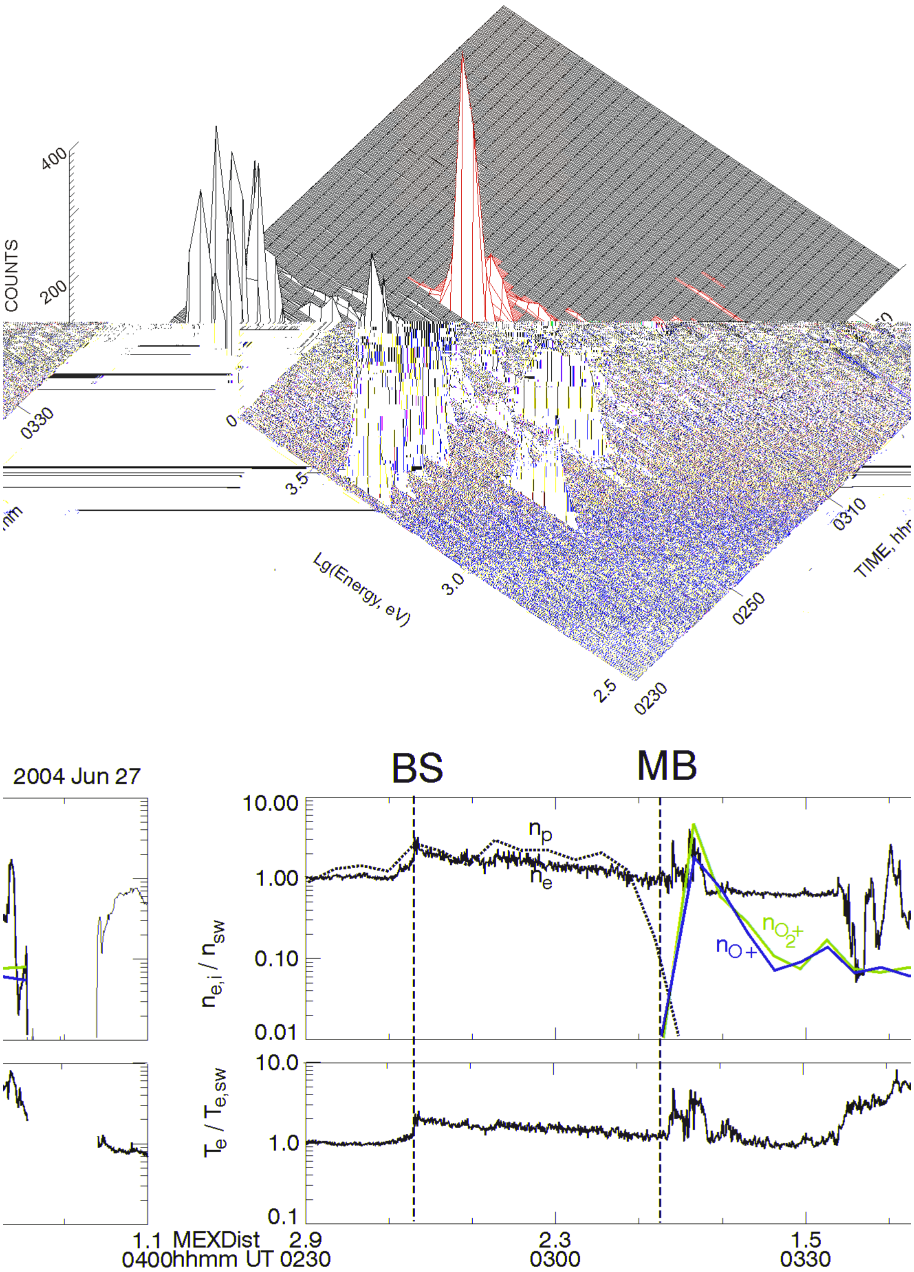

Figure 1.3. (top) Spectrograms of He^{++} (black curves) and O^+ (red curves) ions along the MEX trajectory on June 27, 2004. The oxygen ions dominate in the boundary layer/mantle adjacent to the MB crossed at $\sim$ 0312 UT. (bottom) Variations of the densities of the electrons (the black solid curve), protons (dotted curve), O^+-ions (red curve), O_2^+ ions (blue curve) and the electron temperature. The parameters for the electrons and proton are normalized to the their upstream solar wind values. Note that the electron measurements are carried out at $E_e > 5eV$ (repelling grid). The spacecraft potential also shifts the electron distribution.

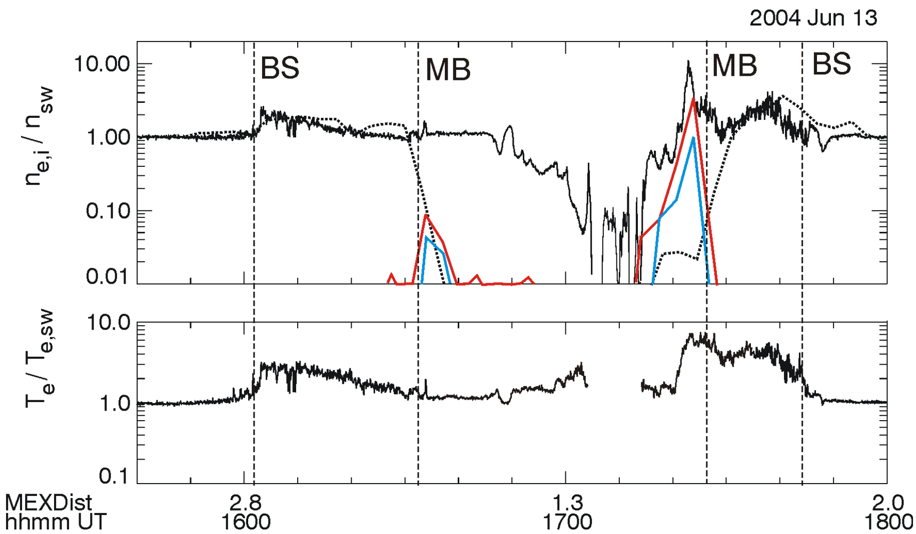

Figure 1.4. The normalized bulk parameters of the electrons and ions along the orbit on June 13, 2004.

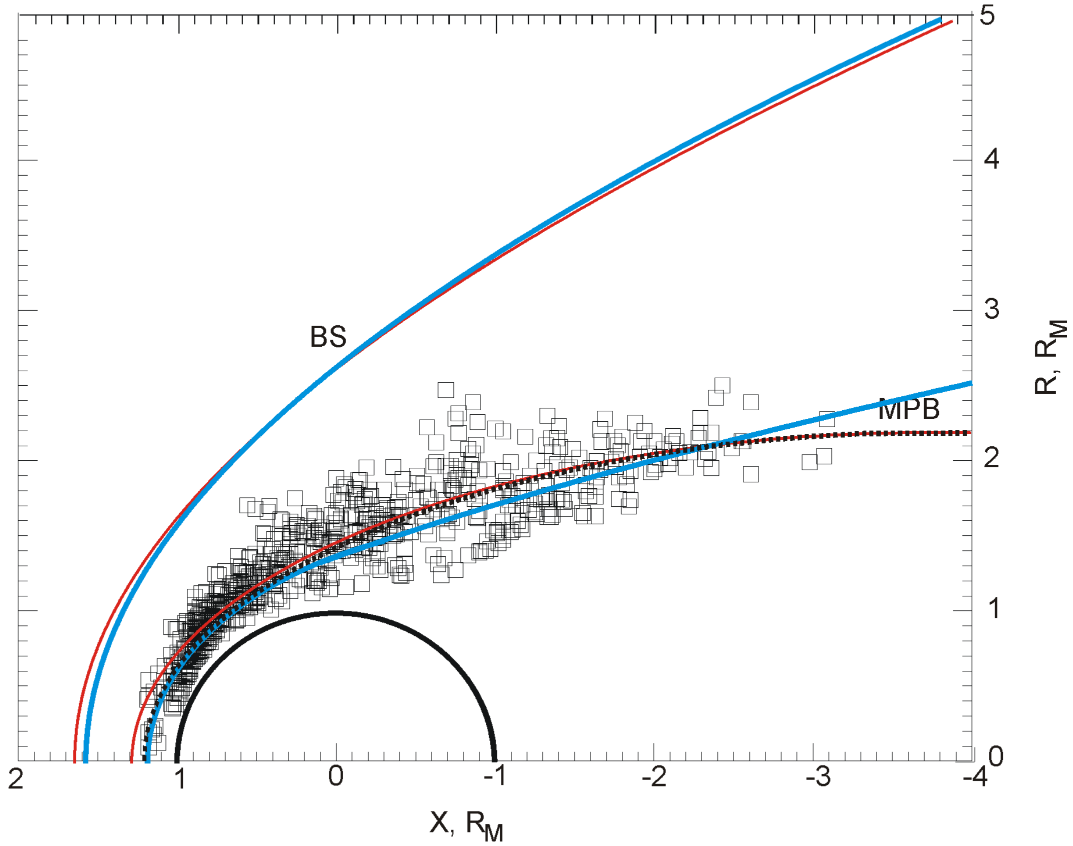

Figure 1.5. Positions of the magnetospheric boundary in cylindrical coordinates. Red and blue curves depict the nominal positions of the bow shock (BS) and the magnetospheric boundary inferred from the MGS and Phobos-2 observations, respectively. The dotted curve presents fits to the ASPERA-3 observations on the MEX orbits.

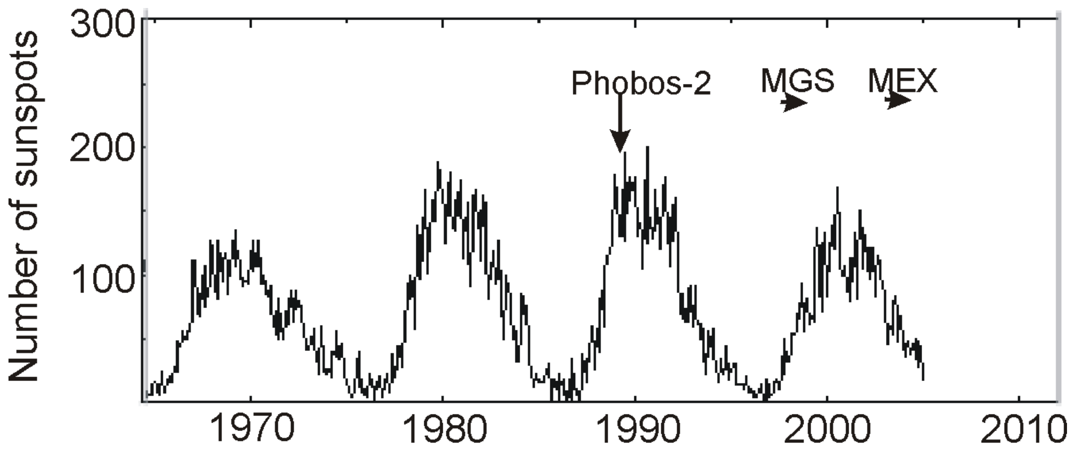

Figure 1.6. Solar cycle variations during the periods when the PHOBOS-2, MGS and MEX observations discussed in this paper were made.

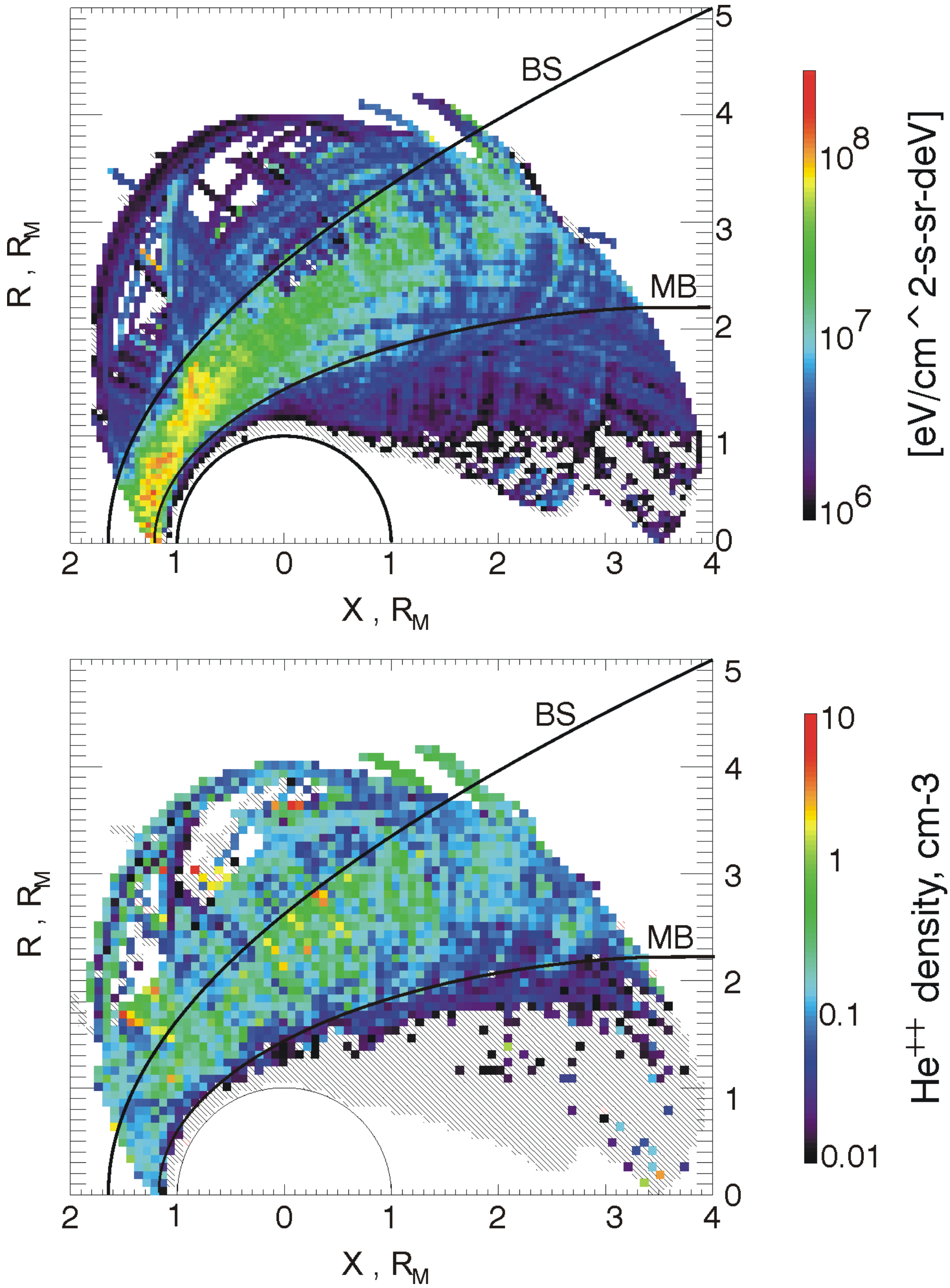

Figure 1.7. Images of fluxes of electrons ($E_e = 80 - 100$ eV) and density of He^{++} ions in cylindrical coordinates plotted on the total of the MEX orbits during 2004-2005. Positions of the MB (the MEX data) and bow shock (BS) are also given.

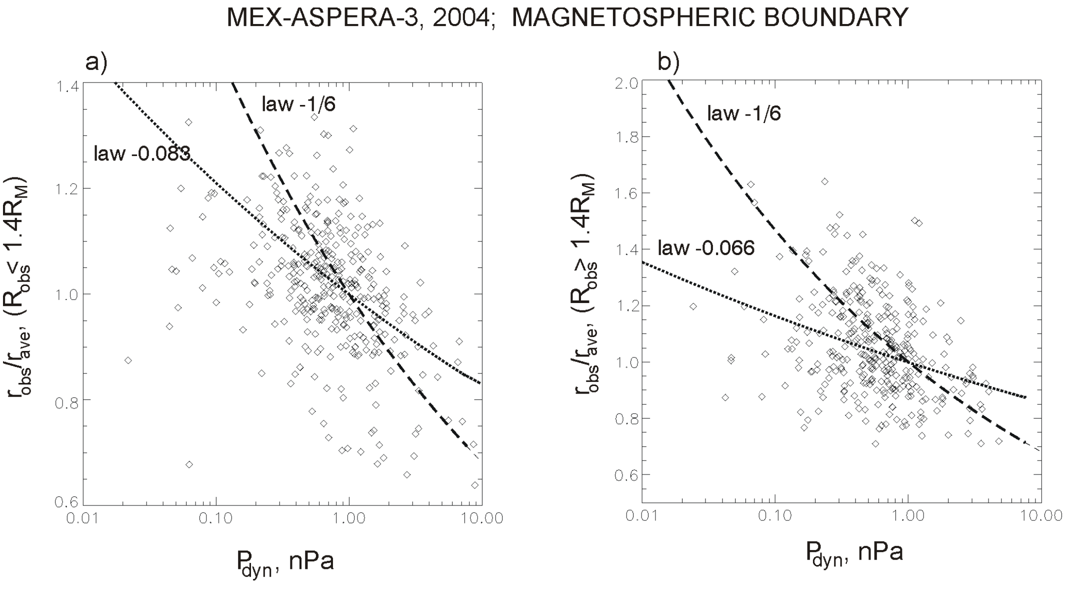

Figure 1.8. Variations in the MB positions as a function of the solar wind RAM pressure. The data are separated on two groups, $R < 1.4R_M$ (a) and $R > 1.4R_M$ (b), where R is a radial distance from the X-axis to the MB crossings. Dashed curves are the power law $P_{sw}^{-1/6}$ dependence. Dotted curves are the power law fits.

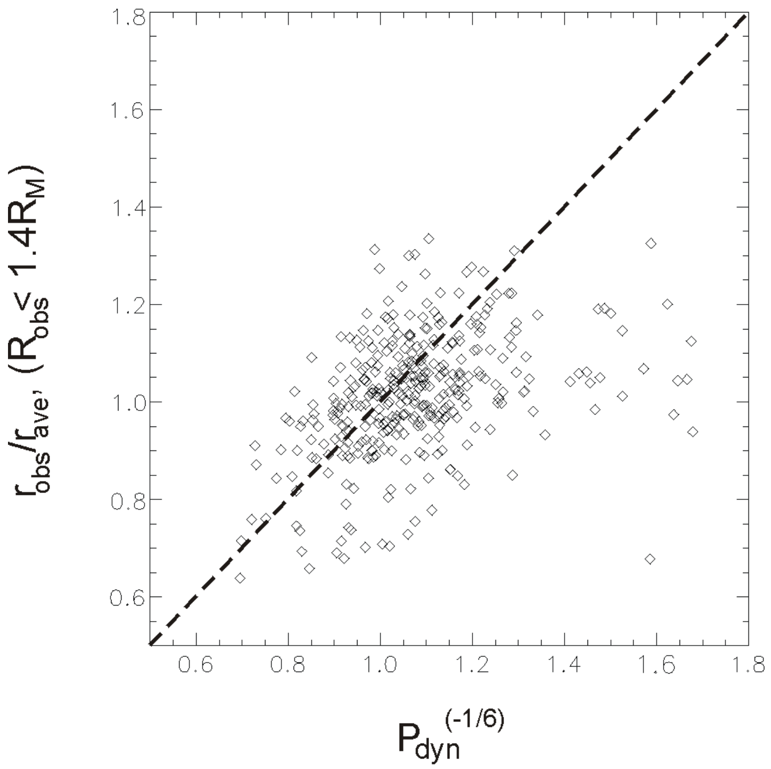

Figure 1.9. Variations in the MB position as a function of $P_{sw}^{-1/6}$

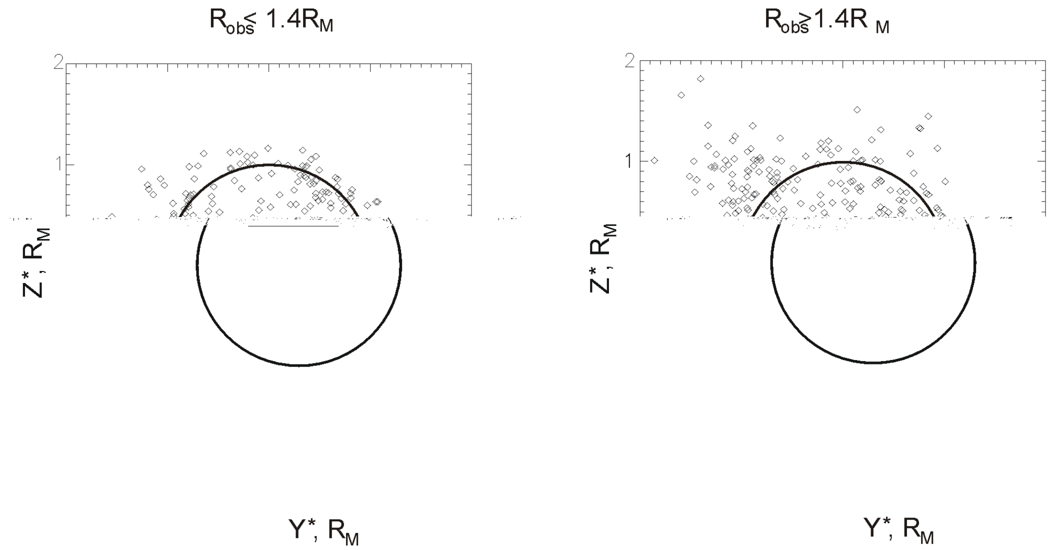

Figure 1.10. Variations in the MB position in the Y^*Z^* -plane, where the Y^*-axis is along the cross-flow component of the IMF, and Z^*-axis is along the motional electric field in the solar wind.

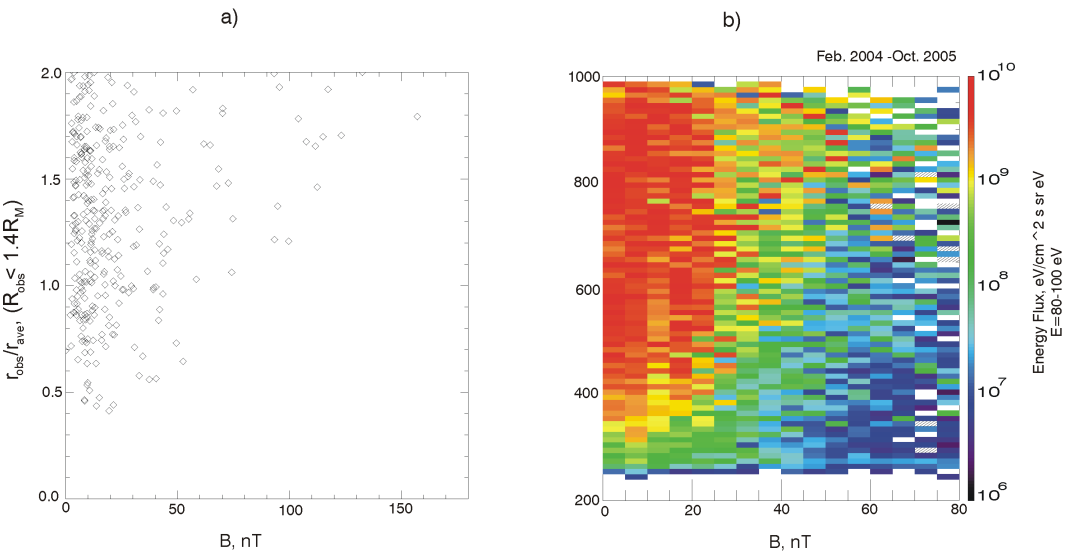

Figure 1.11. (a) Variations in the MB position in the southern dayside hemisphere as a function of the strength of the crustal magnetic field at 400 km. (b) Maximum fluxes of the electrons with $E_e = 80-100$ eV observed at different altitudes during the MEX observations (Feb 2004 -Oct 2005) on the dayside as a function of the magnetic field strength of the crustal sources at altitude of 400 km.

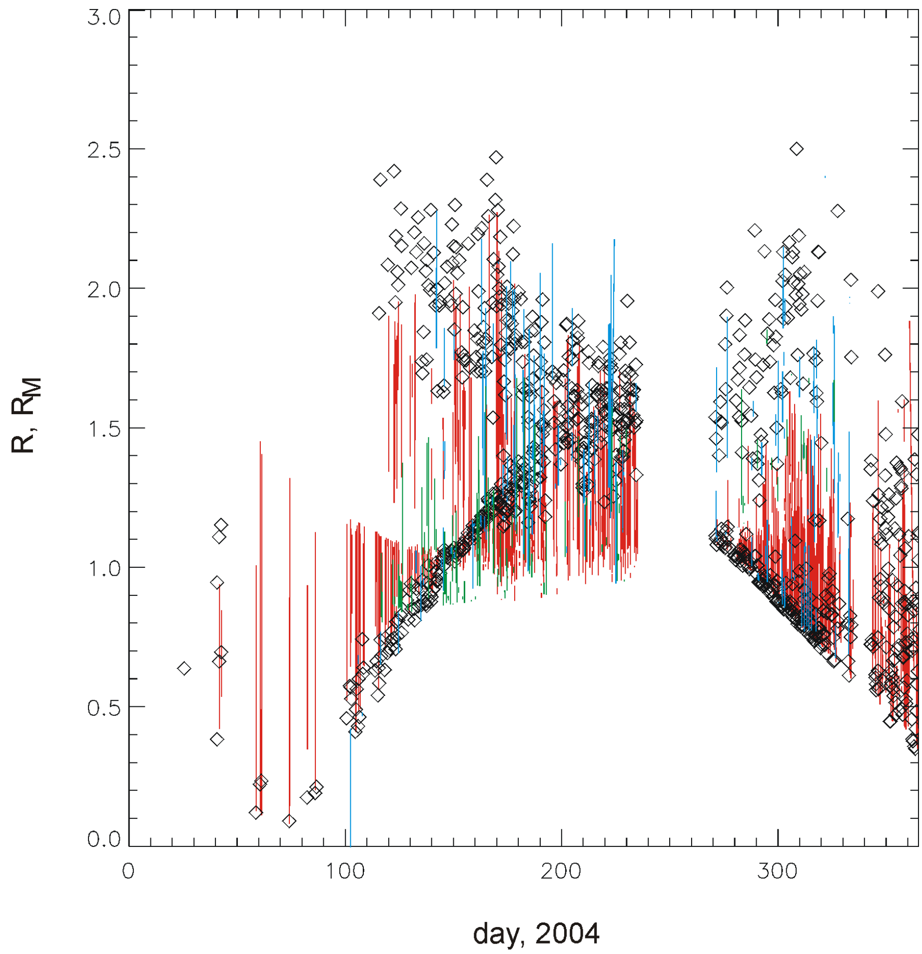

Figure 1.12. Diamond symbols show the radial R positions of the MB on all MEX orbits during 2004 year. The red colored orbital segments depict intervals in which ionospheric photoelectrons were observed. Blue and green segments present the locations of the boundary layer and plasma sheet observations, respectively.

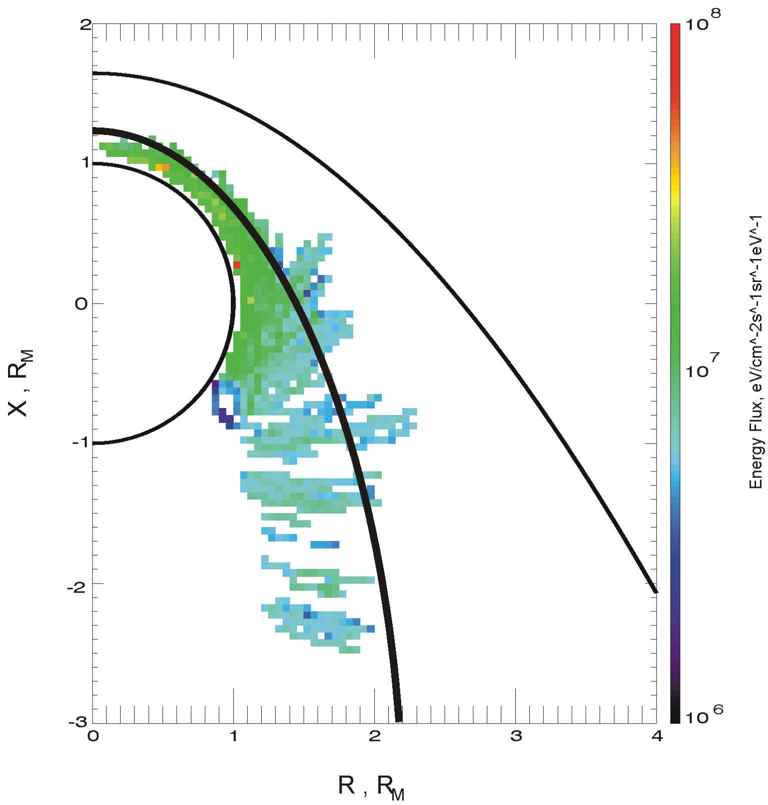

Figure 1.13. Regions in cylindrical coordinates $R-X$ where "CO_2"-photoelectrons were observed. The color shows the energy flux of the photoelectrons.

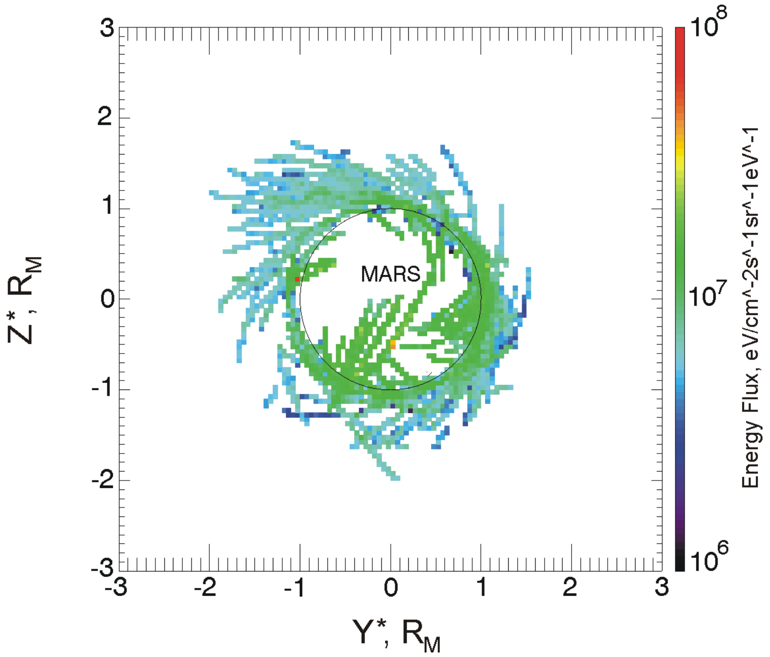

Figure 1.14. Regions in the IMF Y^*Z^* plane where "CO_2"-photoelectrons were observed. The color shows the energy flux of the photoelectrons.

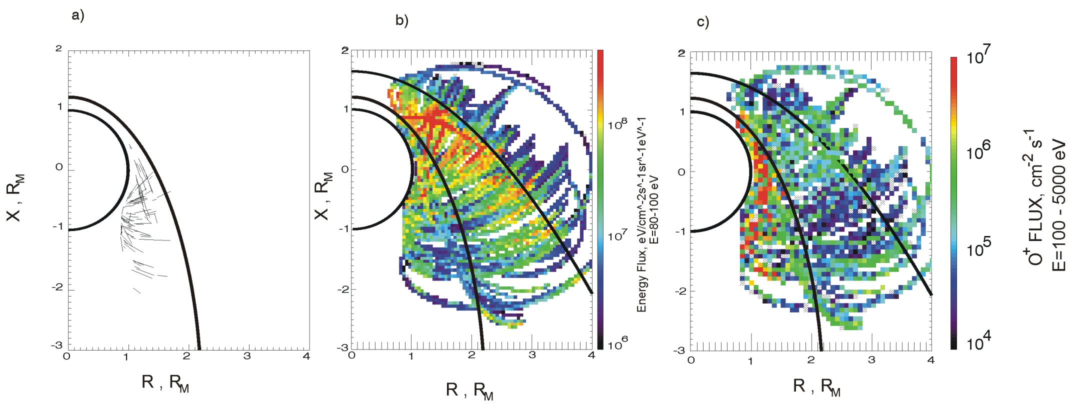

Figure 1.15. (a) Orbital segments in cylindrical coordinates at which electron signatures of the ray-like structures near the wake boundary were observed. (b) The fluxes of electrons with $E_e = 80 - 100eV$ measured on the same set of orbits on which ray structures were detected. (c) Fluxes of oxygen ions on these orbits.

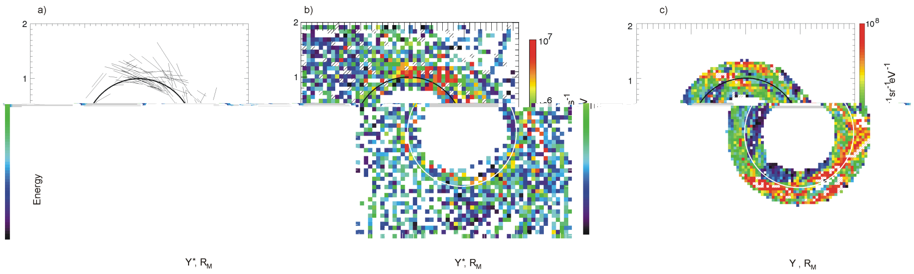

Figure 1.16. (a) Orbital segments in the Y^*Z^*-plane of the IMF coordinate system at which the electron signatures of ray-like structures near the wake boundary were observed. (b) the fluxes of oxygen ions along these MEX trajectories transformed into the IMF reference frame. (c) Maximum fluxes of 80-100 eV electrons in the bins of the ring-area $0.7 - 1.3 R_M$ around Mars for two year observations.

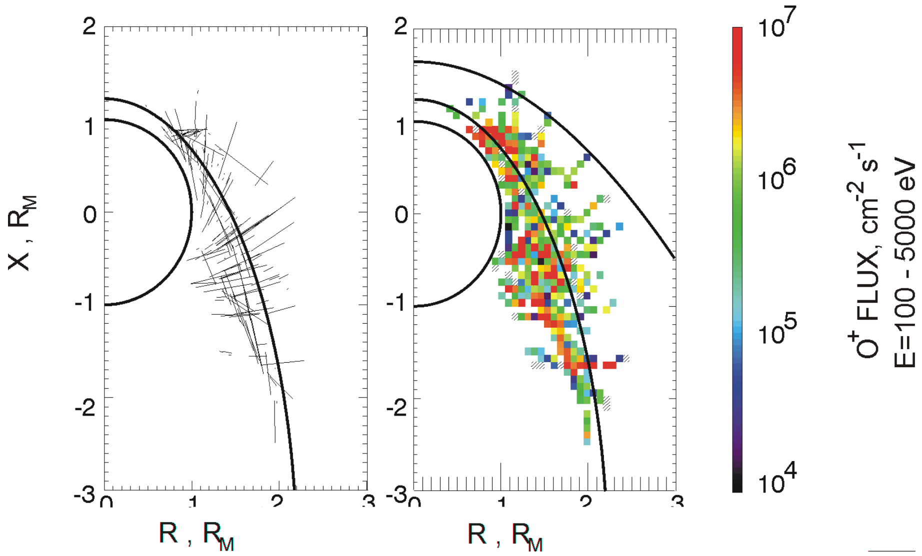

Figure 1.17. Orbital segments in the cylindrical coordinates at which the fluxes of planetary ions were detected in the boundary layer/mantle. The right panel shows the values of oxygen fluxes measured during these intervals.

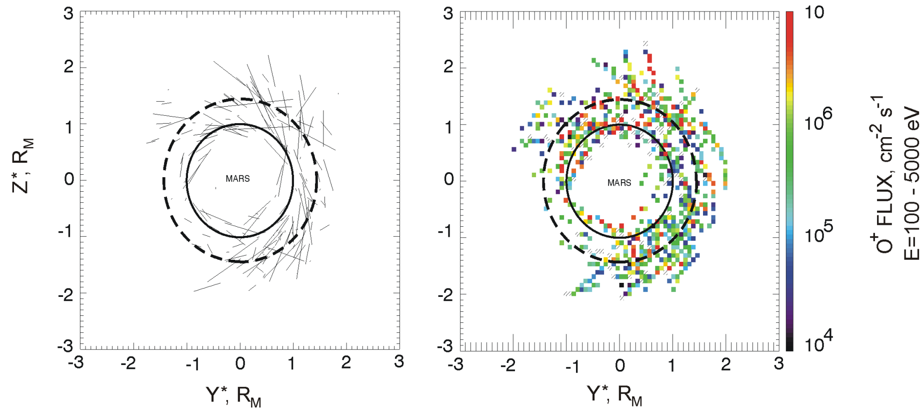

Figure 1.18. Orbital segments in the Y^*Z^* -plane of the IMF coordinate system at which the signatures of the boundary layer were found. The right panel depicts the fluxes of oxygen ions along these orbital intervals.

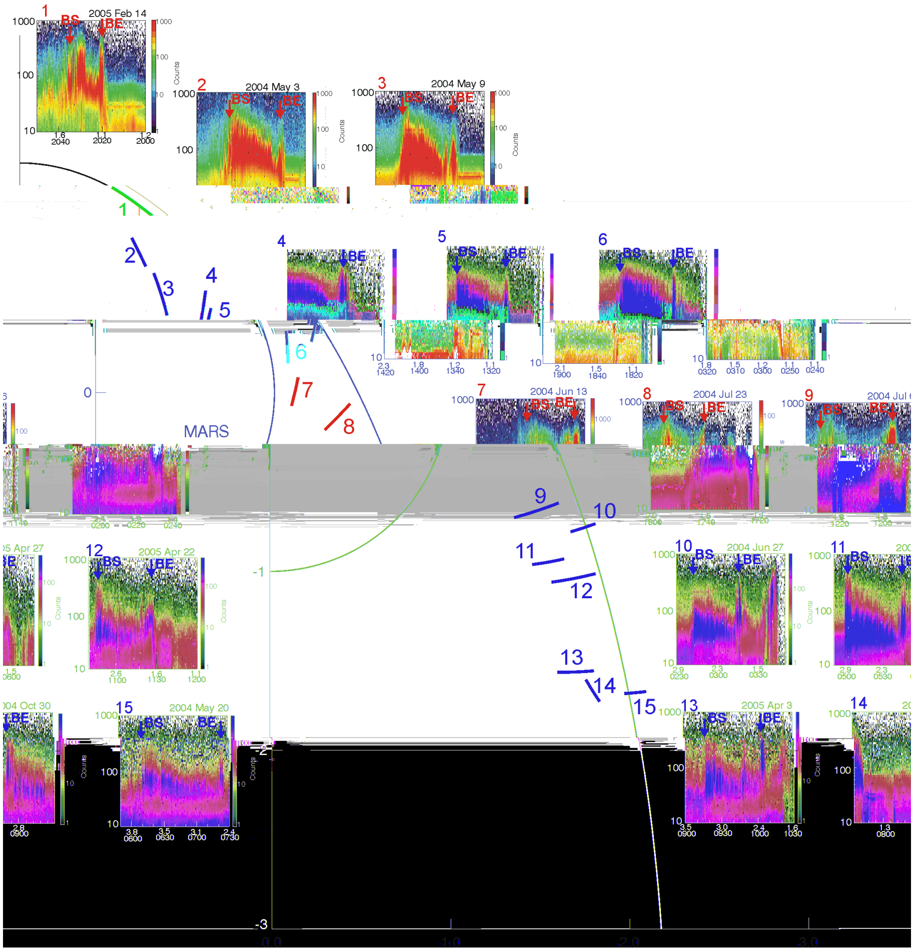

Figure 1.19. Sites near the inner boundary of the magnetosheath where the sheath electrons inhibit an additional heating (boundary events, BE). The spectrograms of electron fluxes which display these events are shown on the small right panels.